Environment, Development and Sustainability (2024) 26:3589–3615
https://doi.org/10.1007/s10668-022-02849-8

Optimization of novel nanocomposite powder for simultaneous removal of heavy metals from palm oil mill effluent (POME) by response surface methodology (RSM)

Anthonette Anak James[1] · Md Rezaur Rahman[1] · Durul Huda[2] · Mohammed M. Rahman[3] · Jamal Uddin[4] · Muhammad Khusairy Bin Bakri[5] · Avishek Chanda[5]

Received: 29 May 2022 / Accepted: 13 December 2022 / Published online: 13 January 2023

Abstract
The treatment of palm oil mill effluent (POME) via adsorption was investigated using a novel nanocomposite powder with the addition of titanium (IV) dioxide (TiO_2) and montmorillonite clay (MMT). Reduced heavy metal content, turbidity, pH, chemical oxygen demand (COD), and total suspended solids (TSS) in POME supported this result. The adsorption processes were carried out in POME with pH 4.4, 658 FAU turbidity, 1256 mg/l COD, and 563 mg/l TSS at a constant mixing speed of 180 rpm for 48 h, with different dosages of adsorbent. The atomic adsorption spectrometry (AAS) analysis revealed that MMT clay was effective in removing lead (Pb) and zinc (Zn) by 86.7 and 97.3%, respectively, aided by the role of activated carbon and photocatalytic behavior of TiO_2 to remove recalcitrant organic pollutants which result in 91.6% reduction in POME turbidity. The final pH value of POME was within the allowable discharged limit as stated in the Environmental Quality Act 1974 (EQA 1974). The response surface methodology (RSM) was modeled based on the COD and TSS analysis results. The findings determined that 1wt% KOH-AC, 0.628wt% TiO_2, and 2wt% MMT clay were the best composition values of novel nanocomposite in showing the most effective reduction of COD and TSS.

✉ Md Rezaur Rahman
rmrezaur@unimas.my

[1] Department of Chemical Engineering and Energy Sustainability, Faculty of Engineering, Universiti Malaysia, Sarawak, Kota Samarahan, Sarawak, Malaysia

[2] Department of Mechanical Engineering and Product Design Engineering, Swinburne University of Technology, Hawthorn, VIC 3122, Australia

[3] Department of Chemistry, Faculty of Science, King Abdulaziz University, P.O. Box 80203, Jeddah 21589, Saudi Arabia

[4] Department of Natural Science, Science and Technology Center, Coppin State University, Baltimore 21216, USA

[5] Composite Materials and Engineering Center, Washington State University, 2001 East Grimes Way, Pullman, WA 99164, USA

Graphical abstract

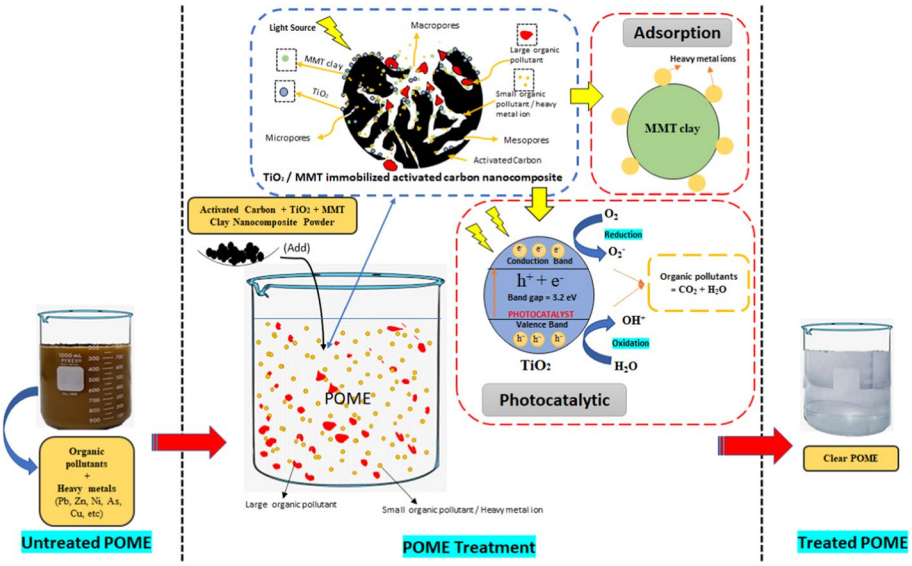

Keywords POME · Adsorption · Respond surface methodology

1 Introduction

Nowadays, the environment has become increasingly affected by the ever-increasing development that simultaneously changes landscapes and pollutes them. Water quality is one aspect of the environment that is frequently impacted because toxic substances such as pesticides, heavy metals, dye, pharmaceutical residues, and organic substances are constantly produced. Moreover, as a result of human activities, it causes effluent discharged to rise in tandem with the growth of the global population, combined with the industrial revolution (Chakravarty & Kumar, 2019; Khan & Ali, 2018; Lellis et al., 2019). According to Edokpayi et al. (2017), one of the primary sources of water pollution is the discharge of massive organic or inorganic contaminants from industries resulting from the waste generation of various manufacturing processes that have been faced ever since the industrial revolution. Indeed, industrial sectors consume a large volume of water in production.

Malaysia, the second largest producer of palm oil in the world, is facing challenges in treating the discharge of palm oil mill effluent (POME) caused by environmental degradation due to the high value of chemical oxygen demand (COD), biochemical oxygen demand (BOD) as well as turbidity rates in water (Kamyab et al., 2018; Osman et al., 2020). Kamyab et al. (2018) mentioned that POME could pollute 100 times more than municipal leachate. POME produced per ton of palm oil ranges between 2.5 and 3.5 tons of effluent production. It is classified as a nontoxic industrial effluent with a brownish color due to the presence of tannin, lignin, pectin, carotene, and phenolic with a water content of 95–96%, oil of 0.6–0.7%, and colloidal suspended solid of 2–4% (Lim et al., 2020; Mohammad et al., 2021). Kamyab et al. (2018) and Mohammad et al. (2021) also

stated that POME emits many methane gases, which potentially cause global warming, and the discharge of POME into waterway reduce oxygen capability in the aquatic environment due to the content of organic and nutrient in POME. Most POME is treated in a traditional ponding system in Malaysia since it has low operating and capital costs. However, some have expressed concern about non-compliance with the Environmental Quality Act 1974 (EQA 1974) discharge limit due to insufficient treatment effectiveness, and the large surface area required because hydraulic retention time (HRT) takes one to two months (Kaman et al., 2017). As a result, treatment measures to mitigate these effects before discharge are required. The adsorption process distinguished a great promise in reclaiming a higher quality of treated POME. However, industries face problems achieving clear crystal water due to POME adsorption (Zahari et al., 2017). Table 1 shows the photocatalytic activity of various photocatalysts for POME degradation.

Photocatalyst	Pollutant	Activator/Condition	Catalyst loading	Band-gap (eV)	Exposure time	Photodegradation performance	Rate of reaction, k (min^{-1})	pH Optimal	References
ZnO	POME	UV light	0.5 g	3.37	5 h 3	COD removal: 30% Color removal: 85% COD removal: 37% Color removal: 70%	n/a	5	Affam and Bistar (2020)
$BiVO_4$	POME	UV light irradiation	1.0 g/L	2.50	4 h	COD removal: 24% for 4 h	1.04×10^{-3}	n/a	Saputera et al. (2021)
TiO_2	POME	UV light (fluorescent tube)	0.01 g/L	n/a	42 min	COD removal: 59.43–96.81% Color: 60.63–94.29%	n/a	5.5	Alhaji et al. (2017)
TiO_2	POME	100 W UV-lamp	5.69wt%	n/a	4 h	Degradation percentage: 63.5% COD removal: 55%	2.90×10^{-1}	8.68	Ng and Cheng (2017)

Table 1 Constraints of the design

Name	Goal	Lower Limit	Upper Limit	Lower Weight	Upper Weight	Importance
A: KOH-AC	Maximize	1	5	1	1	3
B: TiO_2	Maximize	0.1	1	1	1	3
C: Clay	Is in range	0.5	2	1	1	3
TSS	Minimize					
COD	Minimize					

Photocatalyst	Pollutant	Activator/Condition	Catalyst loading	Bandgap (eV)	Exposure time	Photodegradation performance	Rate of reaction, k (min^{-1})	pH Optimal	References
TiO_2 anatase	POME	Solar light	0.1 g/L	3.20	5 h	COD removal: 88.5%	n/a	3.7	Kanakaraju et al. (2017)
ZnO	POME	UV light	1.0 g/L	3.37	22 h	COD removal: 74.12%	n/a	5	Ng et al., (2017)
TiO_2	POME			3.20		COD removal: > 80%			
ZnO-PEG	POMSE	15 W UV-lamp	0.5 g/L	n/a	n/a	COD removal: 94% BOD value: 101 mg/L Turbidity removal:96% Color removal: 73%	n/a	6.5	Zainuri et al. (2018)
$CaFe_2O_4$	POME	Visible light irradiation	0.75 g/L	n/a	8 h	COD removal: 69%	2.71×10^{-3}	8	Charles et al. (2019)

Commercial activated carbon is unquestionably the most used adsorbent for effluent treatment. Activated carbon has an excellent pore structure with a large surface area and a superb adsorption ability to remove organic and inorganic contaminants from wastewater (Ahmad & Azam, 2019; Saleem et al., 2019). Several studies on non-traditional activated carbon for wastewater treatment have been conducted (Popoola, 2019; Reza et al., 2020; Ukanwa et al., 2019). Although commercial adsorbents have good adsorption properties, many issues arise with their disposal that indirectly pollutes the environment. Many studies are recently focusing on low-cost and sustainable adsorbents that are produced from industrial by-products and agricultural waste, as conventional adsorbents have some limitations in terms of cost and regeneration (Chikri et al., 2020; Gisi et al., 2016; Karoui et al., 2019; Maguana et al., 2019). It prompted researchers to seek other natural nonconventional adsorbent materials, for their sustainability and biocompatibility, especially by treating industrial effluent.

Canarium Odontophyllum, also known as Dabai, has been recognized as a possible raw material in activated carbon production. Dabai, a seasonal fruit, is abundantly found in tropical forests in East Malaysia, specifically in Sibu, Sarawak. Hassan et al. (2019) show that several Dabai species are highly valued for their nutritious resins and oil-rich kernels. Dabai can potentially contribute to commercial enhancement, primarily commercial oil, due to its physicochemical properties and nutritional values (Hassan et al., 2019). A rough and woody endocarp of Dabai seed contains edible cotyledon inside, and the physical traits of this nutshell mimic those of a palm kernel shell. Studies related to Dabai nutshell have only recently begun, as it has been discovered that Dabai has strong adsorbent properties. According to Kuang et al. (2020) and Srivatsav et al. (2020), the functional groups present on the surface of Dabai nutshell have a vital role in wastewater adsorption due to their effectiveness in adsorbing multiple ranges of pollutants, such as dyes. Chikri et al. (2020) added that using acid and alkali solutions during the pretreatment of activated carbon-based lignocellulosic materials improved their adsorption properties. However, there is still a scarcity of information on Dabai nutshell activated carbon for wastewater treatment with titanium dioxide (TiO_2) and montmorillonite (MMT) clay. In addition, titanium dioxide (TiO_2) is used due to its inexpensive cost,

low toxicity, excellent chemical stability, high surface-to-volume ratio, and quantum confinement effect. TiO_2 nanopowder provided plenty of active sites for the reactions and improved the catalytic activity due to its large surface area (Reghunanth et al., 2021). The use of clay minerals as an adsorbent and ion exchange for water and wastewater treatment applications, particularly for removing heavy metals, organic contaminants, and nutrients, has surely grown in popularity and use (Lazaratou et al., 2020).

One of the significant shortcomings of previous studies is the failure to indicate the interaction between the process parameters, which necessitates more time and money in multiple trials to achieve optimal effluent discharge values. Hence, this research aims to investigate the efficacy of adsorption processes on various nanocomposite compositions in treating industrial effluent within a short treatment period. To ensure that industrial effluent treatment functions efficiently, titanium dioxide is combined with montmorillonite (MMT) clay-loaded activated carbon in this study to improve adsorption properties and overcome the barriers. In addition, the quality of nanocomposites is examined using several techniques and equipment.

2 Methodology

2.1 Materials

Titanium (IV) oxide (TiO_2) (CAS Number: 14363-67-7), montmorillonite (MMT) K10 (CAS Number 1318-93-0), zinc oxide (CAS Number 1314-13-2) were obtained from Sigma-Aldrich (M) Sdn. Bhd. Dabai (*Canarium odontophyllum*) was obtained from Sibu, Sarawak. Deionized water is obtained from UNIMAS Chemical Laboratory.

The BINDER incubator of the BF Avantgarde (Model BF 56—BINDER Asia Pacific (Hong Kong) Ltd.) with forced convection is used to dry the samples. An LT Furnace was used for the carbonization process. A Panasonic MX-AC 400 Mixer/Grinder (Panasonic Corporation, Kadoma, India) was used to grind the sample before treatment, carbonization, and ball-milling process to assist the process. A Retsch Planetary Ball Mill (Model PM400—Retsch GmbH, Haan, Germany) was used for the ball-milling process. Laboratory apparatus such as steel mold, beakers, conical flask, filter funnels, spatula, glass rod, and precision electronic balance (Model FX-A200i–A&D Company Ltd.) was used during the nanocomposite preparation and treatment process.

2.2 Methods

2.2.1 Raw material collection

Dabai seed was collected from an orchard in Sibu, Sarawak, during the seasonal period. Dabai nutshell was air-dried and stored in an airtight compartment. First, the Dabai seeds were crushed with a pestle and mortar to separate the kernel from the nutshell. Afterward, it was soaked in an acetone solution to remove impurities, and the Dabai nutshell was cleaned with deionized water. Next, the sample was placed in an oven at 110 °C for 24 h to dry. After drying, the sample was crushed and sieved once more to obtain small particles that would increase surface interaction during activation.

2.2.2 Chemical activation of Dabai nutshell

Twenty grams of ground Dabai shell was treated and activated using 100 ml of potassium hydroxide (KOH) in an auto-shaker at 140 rpm for 24 h. After completing the sample activation, the sample was washed thoroughly with deionized water. After obtaining the desired pH value, the sample was placed in the oven to dry at 80 °C for 12 h. The sample was spread on a plate to ensure even heat distribution and to eliminate variable hot pots during the drying process.

2.2.3 Carbonisation of Dabai

The carbonization process was performed using LT furnace. The dried treated Dabai particle was then transferred into a ceramic bowl and wrapped in aluminum foil and a layer of clay before being placed in the LT furnace for carbonization. During the carbonization step, the temperature was ramped from room to 200 °C, followed by 400 °C with a heating rate of 10 °C /min. At 400 °C, the temperature was held for 1 h for the carbonization process. Next, the furnace was cooled at 6.16 °C /min until it reached room temperature. After completing the carbonization process, fine biocarbon was obtained. It was collected and sieved using a 200-µm sieve to reduce the fine biocarbon (or biochar) and assist the ball milling process. The sample was left overnight and retrieved from a furnace the next day.

2.2.4 Ball milling process

To further assist the ball milling process, the fine size of biocarbon (or biochar) obtained was further ground using a grinder for about 5–10 min at speed ranging between 18,000 and 20,000 rpm. It was added into the cylindrical compartment of the ball mill (around 55% of the capacity). Twenty small-size stainless-steel balls of 0.5 g each were used to transform the biochar into a nanosize. The biochar was milled for 30 h, and the sample was extracted for testing periodically at an interval of time to ensure it reached the nanosize level.

2.2.5 Experimental design by response surface methodology

An experimental design is a method for determining factors in research that affect the outcome results. This method maximizes efficiency by reducing process variability and costs, material waste, and labor complexity. RSM (response surface methodology) is a multivariate optimization tool that utilizes mathematical and statistical methods. The RSM refers to the polynomial equation used to study the behavior of the dataset. It investigates the optimal experimental conditions for preparing nanocomposite powder from Dabai nutshell activated carbon, titanium dioxide, and MMT to achieve the best results with the fewest experiments. The statistical software Design Expert® 13.0 StatEase Inc. analyzed the preliminary design.

The nanocomposite preparation parameters were investigated using D-optimal (custom) mixture design, a standard RSM in Design Expert® 13.0 StatEase, Inc. According to Behera et al. (2018), RSM is a suitable method for fitting a quadratic surface and optimizing process parameters with a few experiments while also analyzing the interaction between the parameters. Quantitative data were used to determine the regression model,

followed by response (dependent variable) optimization, influenced by dependent variables. The TSS and COD values were the dependent variables in RSM. In contrast, the independent variables were the weight percentage of Dabai nutshell KOH-activated carbon, TiO_2, and MMT, as shown in Table 1**.** The variations in material composition were generated by the Design Expert® software based on the parameters' limits set in the software, as shown in Table 2. These values were used to prepare nanocomposites for the adsorption of POME contaminants.

2.2.6 Preparation of activated carbon nanocomposite powder

Table 2 shows the Design Expert composition results of Dabai-based activated carbon, titanium dioxide, and MMT to create the nanocomposite powder. Each sample received 40 ml of deionized water to create a suspension sample and stirred for 20 min with a magnetic stirrer.

2.2.7 Collection of palm oil mill effluent (POME) sample

The POME was collected from the effluent pond located at SALCRA Palm Oil Mill Bau, Sarawak, and was put in airtight polyethylene bottles and kept in the refrigerator at 4 °C in the laboratory before performing the adsorption and photocatalytic treatment.

2.2.8 Application of nanocomposite powder for photocatalytic degradation of POME

The solar photocatalytic degradation of POME was performed at the Department of Chemical Engineering and Energy Sustainability, Faculty of Engineering, Universiti

Table 2 Experimental factors

Std	Run	Factor 1 A: KOH-AC (wt%)	Factor 2 B: TiO_2 (wt%)	Factor 3 C: Clay (wt%)
16	1	3	0.55	1.25
3	2	1	1	0.5
2	3	5	0.1	0.5
15	4	3	0.55	1.25
1	5	1	0.1	0.5
10	6	3	1.30681	1.25
4	7	5	1	0.5
8	8	5	1	2
13	9	3	0.55	1.25
9	10	6.36359	0.55	1.25
6	11	5	0.1	2
11	12	3	0.55	2.51134
5	13	3	0.55	1.25
7	14	1	1	2
14	15	3	0.55	1.25
17	16	3	0.55	1.25
12	17	1	0.1	2

Malaysia Sarawak, Malaysia. Each sample of activated carbon nanocomposite powder as designed in Table 2 was placed in a flask containing a 1:1 sample-to-POME mixture and covered with a polyethylene wrap to prevent evaporation. The solar photocatalytic treatments were carried out for 48 h simultaneously with the adsorption treatments, with the samples exposed to a light source during the daytime. The temperature and intensity of sunlight during the daytime, as measured by a portable digital Lux meter (TEX 1335), were recorded on a regular basis. Based on the observation, the temperature and intensity of sunlight ranged from 28 to 27 °C and 30 to 180 Klux, respectively.

2.2.9 Application of nanocomposite powder in adsorption

Batch mode adsorption was used to determine the adsorption capacity of the prepared activated carbon nanocomposite powder suspension. Each sample was placed in a flask containing a 1:1 sample-to-POME mixture. During this process, the flasks were shaken at 180 rpm in a shaker at room temperature for 48 h. The residual concentration was examined using atomic absorption spectrometry (AAS) after the adsorption was completed to investigate the removal of heavy metals from POME. The impurities with the highest adsorption values were chosen for the optimization step. It is also used to identify the mesopores in the nanocomposite powder.

2.3 Characterization

Characterization studies a sample nanocomposite powder's morphological, physical, and chemical properties. Several experiments were carried out using Fourier transform infrared spectroscopy (FTIR), scanning electron microscopy (SEM), energy-dispersive X-ray (EDX), and atomic adsorption spectroscopy (AAS).

2.3.1 Fourier transform infrared spectroscopy (FTIR)

FTIR 'IRAffinity-1' spectroscopy (Shimadzu, Japan) was conducted to examine the functional groups and structures of the molecular bond by analyzing the IR spectrum bands between 4000 and 400 cm^{-1}. The FTIR spectrum results were analyzed using ASTM E1252-98 (2021) and ASTM E168-16 (2016) standards.

2.3.2 Scanning electron microscopy (sem) and energy-dispersive X-ray (EDX)

Hitachi Analytical Tabletop SEM (benchtop) 'TM-3030' (Hitachi High-Technologies (Germany) Europe GmbH.) was used to examine the morphological image data of the samples, particularly the porosity. The samples were positioned on aluminum stubs and fine-coated with a 'JFC-1600' (JEOL (Japan) Ltd.) machine. Images of the composite surface were collected using a field emission gun with 5 and 15 kV voltage values. This procedure was carried out following ASTM E2015-04 (2014) standard. Energy-dispersive X-ray (EDX) is used to determine the elementary composition of materials in the sample.

2.3.3 Atomic adsorption spectrometry (AAS) analysis

Flame AAS 'AA-7000' spectrometer (Shimadzu; Japan) investigated the concentration of elements present in the POME solution after treatment. This analysis measured the wavelength of electromagnetic radiation emitted by a light source using the prepared standard solution. Two different standard solutions, namely zinc (Zn) and lead (Pb), were used as calibration solutions prior based on the required concentration (ppm) from Sigma. The reference electrode was silver/silver chloride, and the carrier gas was high-purity nitrogen gas.

2.3.4 Chemical oxygen demand (COD) measurement

A closed water sample is incubated with a strong chemical oxidant under specific temperature conditions and for a particular period. The amount of oxidant consumed is expressed in its equivalence to oxygen. Potassium dichromate ($K_2Cr_2O_7$) and boiling sulfuric acid (H_2SO_4) is commonly used as an oxidant in COD assays. 2.0 ml of POME solution and distilled water were added into two different vials. The distilled water was spared as a blank sample. The vials caps were closed tightly, and both vials were shaken gently to mix the contents. The vials were placed in a COD digester (DRB200 Reactor) for the heating process. The temperature was set at 150 °C for 2 h. The vials were removed after 2 h from the COD digester and were cooled at room temperature. The COD values were measured by using HACH DR900. The measurement of the COD was recorded.

2.3.5 pH measurement

The pH measurement materials needed are listed in Table 3.

2.3.6 Total suspended solid (TSS) measurement

Ten milliliters of deionized water was poured into a sample cell and acted as a blank sample to calibrate the TSS reading to 0.00 mg/L; 10 ml of raw POME was poured into a sample cell following the calibration. It was wiped clean before inserting the sample cell into the cell holder. Then, the 'read' button was pressed to measure the TSS value of the sample. This procedure was repeated for all samples of treated POME.

Table 3 The materials required for pH measurement

Materials	Detail
Buffer solution	To calibrate the pH meter
pH meter	To measure the pH of the POME
Distilled water	To rinse the pH meter after the measurement of POME

2.3.7 Turbidity measurement

Ten milliliters of deionized water was poured into a sample cell and acted as a blank sample to calibrate the turbidity reading to 0.00 FAU; 10 ml of raw POME was poured into a sample cell following the calibration. It was wiped clean before inserting the sample cell into the cell holder. Then, the 'read' button was pressed to measure the turbidity value of the sample. This procedure was repeated for all samples of treated POME.

3 Results and discussion

3.1 Initial condition of POME

Initially, the untreated raw POME has a dark brownish color, is highly oily and dense, and has an unpleasant odor. The untreated raw POME has a COD of 1256 mg/L and a pH of 4.4. The pH value is validated because Kaman et al. (2017) found that the initial pH of POME is 4.2. Meanwhile, the total suspended solids (TSS) total is 563 mg/L with a turbidity of 738 FAU. Table 4 summarizes the POME discharge parameters stated in the Environmental Quality Act (EQA) of 1974.

3.2 FTIR analysis of AC/TiO_2/MMT nanocomposite powder

Figures 1 and 2 show the FTIR results for the developed AC/TiO_2/MMT nanocomposite powder before and after treatment with palm oil mill effluent (POME). The adsorption band at 1600.92 cm^{-1}indicates C=C stretching of conjugated and cyclic alkene, which can be observed in Fig. 1 of nanocomposite powder before the adsorption process occurs. The peak intensity at 1203.58 cm^{-1} in Fig. 1 and 1207.44 cm^{-1}in Fig. 2 shows the adsorption peak of a strong C–O stretching band of alkyl aryl ether, while the peak at 1035.77 cm^{-1} distinguished a strong S=O stretching in AC/TiO_2/MMT nanocomposite powder before adsorption process (Fig. 1). This peak is also observed in Fig. 2 of AC/TiO_2/MMT nanocomposite powder after POME treatment. According to Chobchun et al. (2020) and

Table 4 Standard discharge parameters for POME (Shahrifun, 2015) and the initial conditions of the POME sample

Parameter	Standard limits for POME	Initial conditions of POME
Biological oxygen demand (BOD) (mg/l)	100	–
Chemical oxygen demand (COD) (mg/l)	–	1256
Total solids (mg/l)	–	–
Suspended solids (mg/l)	400	563
Oil and grease (mg/l)	50	–
Ammoniacal nitrogen (mg/l)	150	–
Total nitrogen (mg/l)	200	–
pH	5–9	4.4

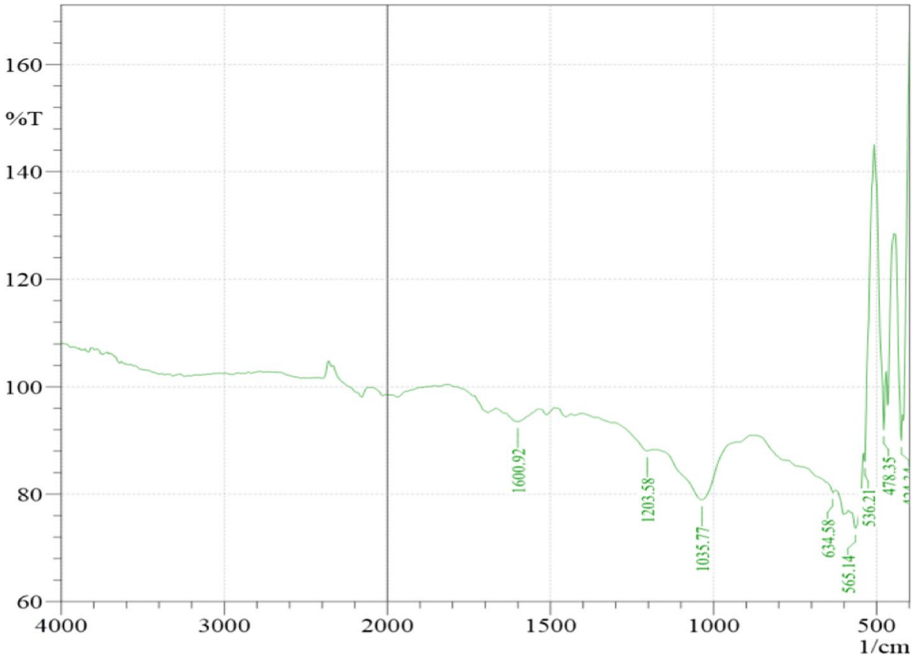

Fig. 1 IR spectra of AC/TiO_2/MMT nanocomposite before adsorption

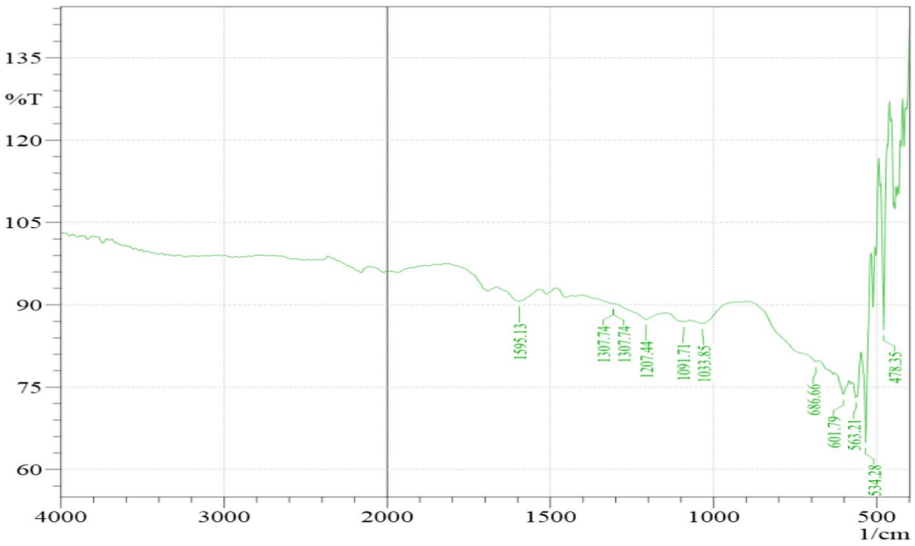

Fig. 2 IR spectra of AC/TiO_2/MMT nanocomposite after adsorption

Kusiak-Nejman et al. (2018); the peak between 1038 and 1060 cm^{-1}represents C and Ti–O electron affinity, indicating the incorporation of carbon into titanium dioxide.

The absorption peak at 1091.71 cm^{-1}, as in Fig. 2 indicates the C–O stretching for secondary alcohol. The peak at 634.58 cm^{-1} refers to the C–Cl stretching band of the halo compound. The appearance of peak intensity at 565.14 and 536.21 cm^{-1} in Fig. 1 and 563.21 and 534.28 cm^{-1} in Fig. 2 represents the Si–O stretching variation bond MMT nanofiller. Such peaks also have been observed in the study of POME treatment using silica membrane and poly(L-lactic acid)-poly (ethylene glycol) conducted by Kamil et al. (2020). The presence of these peaks provides a good adhesion interaction between the nanocomposites. Arjmandi et al. (2016) and Adeleke et al. (2017) reported that MMT has several uniform polar sites on its structure that indicate the content of electron density along with the interlayer spaces and their surfaces. As stated by Kuang et al. (2020) and Ahrouch et al. (2019), the addition of MMT clay has little effect on the chemical composition, but it lowers the adsorption peak of activated carbon. It is supported by the findings of Arjmandi et al. (2016). They discovered that the chemical structure of MMT clay with nanocomposite does not change because no new functional groups are observed. The IR absorbance band for 1307 cm^{-1} in Fig. 2 represents the functional group of either C–O stretching or S=O stretching for the sulfone group. When comparing Figs. 1 and 2, the intensity of the peaks shifts to a slightly higher and sharper peak for the nanocomposites after the POME adsorption process.

Figures 1 and 2 show nearly identical results to the FTIR results obtained by Taoufik et al. (2019). The characteristics of the Ti–O–Ti functional group are shown by peaks ranging from 780 to 600 cm^{-1}, with the peak at 478.35 cm^{-1} illustrating the Ti–O bands. These findings are supported by the FTIR result obtained by Leon et al. (2016) and Mannaa et al. (2021), which show that the peak of 470 cm^{-1} is attributed to the Ti–O group. In addition, TiO_2 attachment on the AC surface resulted in the 1080 cm^{-1} peak formation (Tian et al., 2016). A similar peak also appeared in Fig. 2 at 1091.71 cm^{-1}. According to Fausey et al. (2019) and Pant et al. (2020), the peak intensity between 700 and 420 cm^{-1} is attributed to Ti–O vibration, which explains the interaction between biomass and TiO_2.

3.3 Scanning electron microscopy (SEM) and energy-dispersive X-ray (EDX) analyses before and after POME treatment

Figure 3A and b shows the distribution of sample 13 nanocomposite in removing contaminants from POME at × 200 and × 1000 magnifications, respectively. Meanwhile, Fig. 3c and d shows the morphological result of sample 17. Eskandari et al. (2019) show that a high TiO_2 to AC ratio produces a positive response compared to a lower TiO_2 composition. However, both chosen samples have lower TiO_2 values than AC. According to the observations, numerous affected areas in Fig. 3a and b could be contaminants' adsorption efficiency. The white affected area in Fig. 3a, b, c, and d represents pollutants on the micropores of AC with a combination of TiO_2 and MMT particulates. The results show that increasing the amount of AC increases the ability of contaminants to adsorb. For this reason, a large proportion of porous structured AC has micro- and mesopore structures that promote high adsorption capacity (James et al., 2022). The results of the turbidity test and the pH value of sample 13 support this assertion.

The EDX analysis confirmed the presence of titanium on the surface of carbon, as shown by the SEM analysis. Figures 4 and 5 show the element composition peaks in samples 13 and 17 AC/TiO_2/MMT clay nanocomposites after POME treatment. Carbon (C)

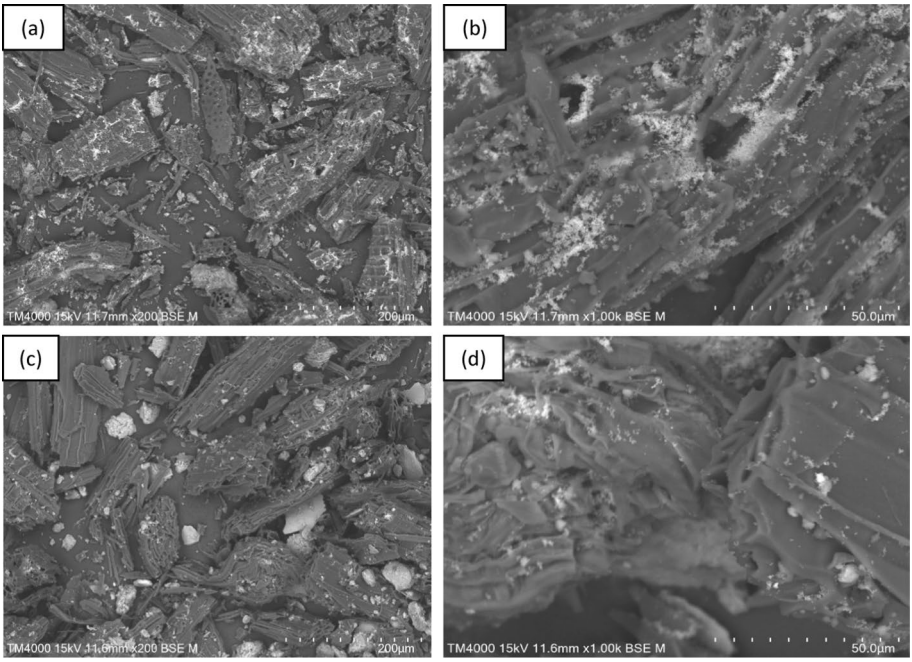

Fig. 3 Morphological images of the sample (**a**) 13 nanocomposites after POME treatment (×200 magnification), (**b**) 13 nanocomposites after POME treatment (x1k magnification), (**c**) 17 nanocomposites after POME treatment (×200 magnification), (**d**) morphological image of sample 17 nanocomposites after POME treatment (x1k magnification)

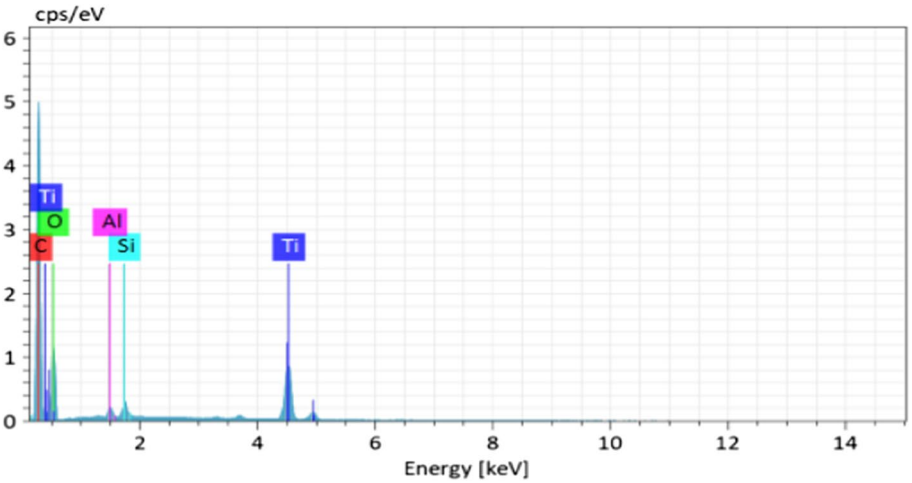

Fig. 4 Energy-dispersive X-ray (EDX) diffraction spectra with its element compositions of sample 13 (treated)

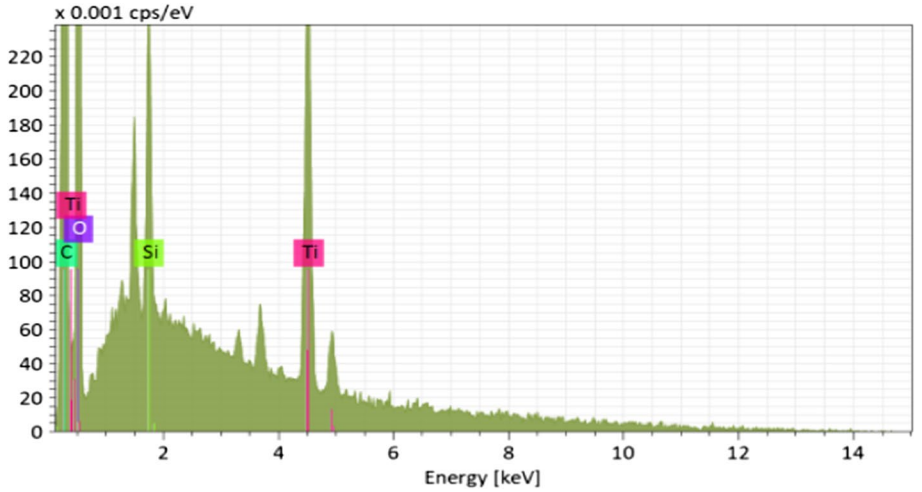

Fig. 5 Energy-dispersive X-ray (EDX) diffraction spectra with its element compositions of sample 17 (treated)

Table 5 EDX composition of sample 13 (treated)

Element	Mass (%)	Atom (%)	Abs. error (%) (σ)	Rel. error (%) (σ)
C	69.4628	70.2157	8.0177	11.5424
O	33.9787	25.7848	4.4562	13.1147
Ti	12.8457	3.2574	0.4053	3.1548
Si	1.0733	0.4640	0.0741	6.9067
Al	0.6181	0.2782	0.0583	9.4302

Table 6 EDX composition of sample 17 (treated)

Element	Mass (%)	Atom (%)	Abs. error (%) (σ)	Rel. error (%) (σ)
C	74.2719	80.8970	8.5038	11.4496
O	21.9708	17.9651	3.1217	14.2083
Ti	3.1794	0.8687	0.1281	4.0305
Si	0.5779	0.2692	0.0532	9.2116

and oxygen (O) have the highest atom percentage of elements based on the EDX spectrum presented by the graphs since carbon is the major component of carbonaceous material. According to the tables, the C percentage for Table 5 is 69.4628%, whereas Table 6 shows 74.2719% of carbon. The oxygen (O) percentages are 33.9787% in Table 5 and 21.9708% in Table 6. According to the findings, the carbon content of sample 13 is slightly lower than sample 17, while the oxygen content of sample 13 is somewhat higher than sample 17. This variation could be attributed to the uneven distribution of elements in the samples.

Other elements discovered in samples include silicon (Si) and aluminum (Al). Table 5 shows a much higher percentage of Ti (12.84%) than Table 6, which is 3.17%. Again, this is due to the uneven distribution of Ti on the carbon surface, with some points having high Ti concentrations. Impurities can be seen in the EDX spectra, most notably aluminum (Al), while the presence of Si corresponds to the Dabai nutshell element. Mopoung et al. (2015) researched the preparation of KOH-activated carbon using tamarind seeds, which included both elements.

3.4 Atomic adsorption spectrometry (AAS) analysis for heavy metal

Even in small amounts, the discharge of heavy metals into the water bodies causes serious environmental issues because of their toxic nature (Briffa et al., 2020; Jagaba et al., 2020). It causes not only environmental problems but also impacts humans. Lead and zinc are examples of heavy metals found in the POME sample that must be removed before the POME is discharged into the water. Figure 6 depicts the final heavy metal content in the POME solution after treatment using different AC/TiO_2/MMT clay compositions, as recorded in Table 2. The initial Zn concentration is 2.4 ppm, while the initial Pb concentration is 3.5 ppm.

According to the observations, the highest concentration of Zn is found in sample 3, with 0.7949 ppm. The highest concentration of Pb is found in sample 8 with 0.37082 ppm, where the AC/TiO_2/MMT composition ratios are 5:0.1:0.5 and 5:1:2, respectively. On the other hand, the samples with the lowest Zn and Pb concentrations are sample 7 (0.3192 ppm) and sample 1, 6, 9, 15, 16, 17, which all have the same Pb concentration of 0.0945 ppm. Therefore, samples 1, 9, 15, 16, 17 all have an equal amount of AC/TiO_2/MMT composition. Adeleke et al. (2017) stated that increasing the amount of activated

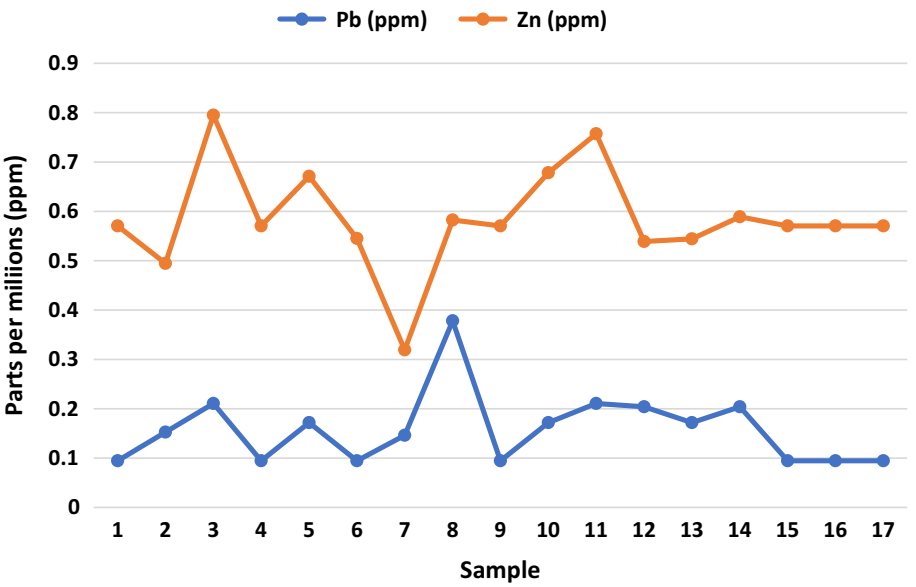

Fig. 6 The concentration of Zn and Pb in POME after treatment

carbon will increase heavy metal removal. Adeleke et al. (2017) also reported that at 20 g of adsorbent dosage, Zn adsorption from POME solution could achieve up to 94.68%. This statement supported the findings that 5wt% AC with 1wt% TiO_2 and 0.5wt% MMT in sample 7 can reduce up to 86.7% of Zn ion from POME at 6.5 g of adsorbent dosage. Meanwhile, when adsorbents from samples 1, 6, 9, 15, 16, and 17 are applied to the POME solution, a 97.3% reduction in Pb is achieved.

This high adsorption capacity is due to the presence of many pore spaces on the surface of activated carbon, which allows heavy metal ions to attach. The particle distribution on the developed nanocomposite sample after POME treatment can be observed in Fig. 3. In addition, Osman et al. (2020) and Adeleke et al. (2017) studied other factors influencing heavy metal uptake from POME samples: treatment temperature and contact time. According to Chikirida et al. (2019), Abu-Danso et al. (2019), and Akhbarizadeh et al. (2018), combining MMT clay with biocomposite increases heavy metal adsorption capacity from an aqueous solution.

3.5 Measurement of turbidity and pH

Turbidity is a measurement of sample cloudiness caused by suspended particulates such as inorganic and organic matter (Bozorg-Haddad et al., 2021; Scholz, 2016). The POME sample has an initial turbidity concentration of 658 FAU with a pH of 4.4. Treatment is performed on 17 AC/TiO_2/MMT clay samples with varying composition values, as tabulated in Table 2. The developed nanocomposites are applied to POME samples to study the effectiveness of their performance in POME treatment with a contact time of 48 h at 180 rpm, where the result is tabulated in Fig. 7. Based on the observation, the lowest turbidity value of POME is 155 FAU by sample 5, with a composition ratio of 1:0.1:0.5.

In comparison, sample 8, with a composition ratio of 5:1:2, has the highest turbidity value of 533 FAU. Sample 5 nanocomposite reduces turbidity concentration by approximately 91.6%. The dosage of nanocomposite powder has significantly influenced the turbidity of POME, as evidenced by the result of sample 8. Clouded POME solution reduced light penetration in TiO_2 photocatalyst, thereby affecting the production of highly reactive radical species of superoxide (O_2^-) and hydroxyl (OH^+) that are responsible for catalytic

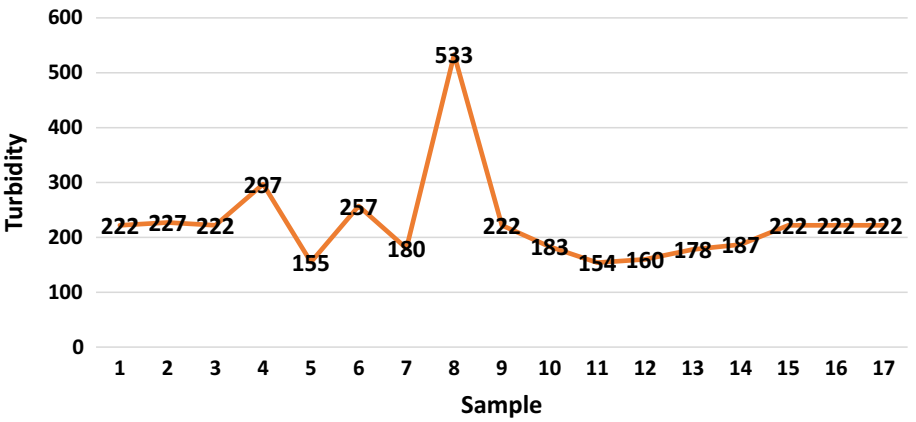

Fig. 7 Effect of AC/TiO_2/MMT clay nanocomposite on POME turbidity

oxidation of organic pollutants into CO_2 and H_2O (Bansal et al., 2019; Bui et al., 2019). Furthermore, the difficulty of light penetration into TiO_2 has resulted in a reduction in charge carrier generation during photocatalytic reactions (Nguyen-Dinh et al., 2021). Compared to other researchers' results, the treatment is feasible, and the outcome is nearly identical to the POME turbidity treatment performed by Amosa et al. (2016). Amosa et al. (2016) investigated the efficacy of EFB in reducing POME turbidity under constant conditions of 3.5 g powdered activated carbon/100 ml biotreated POME with a contact time of 45 min and agitation 150 rpm. Compared to Sia et al. (2016) research on the study of POME treatment with coconut shell AC (acid-washed), the application of the developed nanocomposites is far more applicable in decreasing POME turbidity. The synergistic effect of TiO_2 and MMT clay facilitates the use of activated carbon in the degradation of organic pollutants and heavy metals from POME. The high surface area of fine-grained MMT clay and TiO_2 offered more vacant active sites as the pores increased, further improving the surface contact interaction between the active site of nanocomposite powder and pollutants. Deprotonation of charge on the surface of the nanocomposite powder occurred at an initial pH of 4.4, promoting more adhesion attraction of pollutants to deposit into the pores of the nanocomposite powder and improving the POME pH value.

The pH parameter is chosen as one of the components assessed under the Environmental Quality Act (EQA) 1974. Before being discharged into the river, the POME must meet the discharged limit established by EQA 1974, which states that the acceptable range for POME is between 5 and 9. According to the results shown in Fig. 8, the pH values for all samples are higher than the initial pH value of POME. The pH values indicate that the POME changes from acidic to neutral after POME treatment. As the pH value of POME approaches neutral, more contact interaction occurs between the pollutants and nanocomposite particles due to no repulsive forces between the neutral surface-charge adsorbent and pollutants (Azadi et al., 2020). Numerous OH ions are generated via oxidation at alkaline conditions which favor the formation of hydroxyl radical species in POME and enhance the rate of organic pollutant degradation. However, at high alkaline conditions, the adsorption rate will be reduced due to electrostatic repulsion between the adsorbent and organic molecules as the surface charge of the organic molecule changes from positive to negative (Bui et al., 2019). Therefore, it is safe to discharge into the river within the normal limit range.

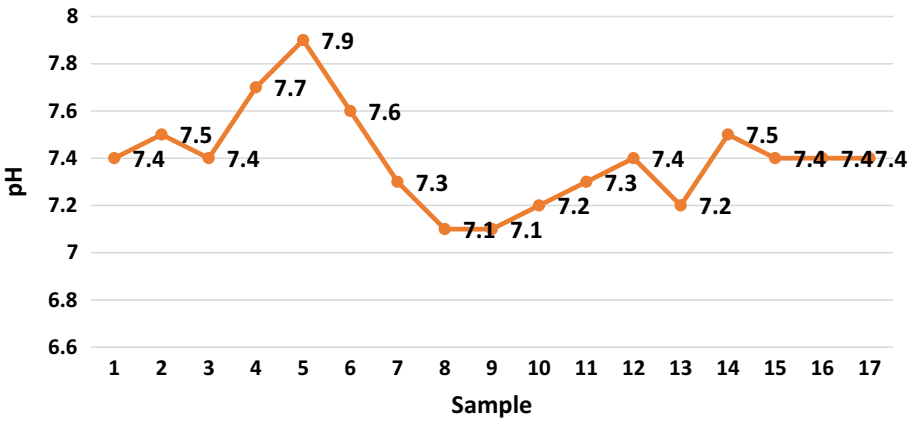

Fig. 8 Effect of AC/TiO_2/MMT clay nanocomposite on POME pH

According to Mohammed (2015), the pH value of the sample and the turbidity result are correlated. A high pH value results in high turbidity removal, as shown in Figs. 7 and 8. Koohestanian et al. (2008) stated that high pH could initiate sedimentation due to conductive alkali conditions. However, according to Kothari et al. (2017), turbidity removal is not the primary influence because the two factors have very low insignificant positive correlations.

3.6 Design of AC/TiO_2/MMT clay nanocomposite powder based on COD and TSS analysis

For the optimization, tests are conducted on all the samples generated by the Design Expert software, as shown in Table 2. Table 7 depicts the developed composite samples with various material compositions tested on their ability to treat POME solutions. Seventeen samples are prepared and used to adsorb contaminants from the POME solution, and their COD and TSS values are determined.

3.7 Effect of analysis of variance (ANOVA) on COD and TSS analysis

All samples are subjected to COD and TSS tests, and the results are inserted into the design expert software for further data analysis, including ANOVA. ANOVA is used to investigate the effect of parameter changes on COD and TSS, where a conclusion can be drawn based on the experimental data. The value of *P*, which is supposedly less than 0.05, illustrates the significance of the parameter to the model.

Table 7 Experimental design, responding chemical oxygen demand (COD), and total suspended solid (TSS)

Std	Run	Factor 1 A: KOH-AC (g)	Factor 2 B: TiO_2 (g)	Factor 3 C: Clay (g)	Response 1 TSS (mg/l)	Response 2 COD (mg/l)
16	1	3	0.55	1.25	119	635
3	2	1	1	0.5	130	639
2	3	5	0.1	0.5	156	659
15	4	3	0.55	1.25	119	635
1	5	1	0.1	0.5	127	639
10	6	3	1.30681	1.25	135	642
4	7	5	1	0.5	115	631
8	8	5	1	2	167	687
13	9	3	0.55	1.25	119	635
9	10	6.36359	0.55	1.25	145	667
6	11	5	0.1	2	112	629
11	12	3	0.55	2.51134	91	609
5	13	1	0.1	2	40	500
7	14	1	1	2	103	615
14	15	3	0.55	1.25	119	635
17	16	3	0.55	1.25	119	635
12	17	3	0.55	1.25	119	635

Table 8 ANOVA results for COD analysis

Source	Sum of squares	Mean square	*F* value	*P* value
Model	23,356.29	2595.14	165.58	< 0.0001
A-KOH-AC	6005.35	6005.35	383.15	< 0.0001
B-TiO_2	2763.28	2763.28	176.30	< 0.0001
C-Clay	2581.45	2581.45	164.70	< 0.0001
AB	903.13	903.13	57.62	0.0001
AC	4465.12	4465.12	284.88	< 0.0001
BC	5050.12	5050.12	322.21	< 0.0001
A^2	114.93	114.93	7.33	0.0303
B^2	429.86	429.86	27.43	0.0012
C^2	14.82	14.82	0.9457	0.0363
$R^2 = 0.9953$	Adjusted $R^2 = 0.9893$		Predicted $R^2 = 0.8132$	

Based on Table 8, all *P* values are less than 0.05, indicating that all the AB, AC, BC, A2, B2, and C2 are significant to the model. The fit statistic design provided by the software shows that the design has an R^2 value of 0.9953, indicating that the model is well-fit to the experimental data. The adjusted R^2 is 0.9893, and the predicted R^2 is 0.8132. The predicted R^2 of 0.8132 is in reasonable agreement with the adjusted R^2 of 0.9893, where the difference between these values is 0.1761, showing that the model is excellent because the values are less than 0.2. Based on Daneshpayeh et al. (2016), increasing the number of independent variables in the model can improve R^2, but the goodness of fit cannot be determined solely by the value of R^2.

Meanwhile, the adjusted R^2 only increases when there is a strong correlation between the dependent variables. Predicted R^2 shows how well the model generates responses for new findings and the complexity of the model. As a result, adjusted and predicted R^2 are more desirable parameters for the goodness of fit in statistics. The R^2 values in this design are close to one, indicating that the developed models are very significant. Equations (1) and (2) are generated based on the analysis and coded factors of + 1 for high level and −1 for COD and TSS. These equations are used to calculate the predicted values in Table 9**.** Figures 9 and 10 depict the residual plots of experimental values versus COD and TSS. The data showed a straight line with a normal distribution, implying that the data were reliable.

$$\begin{aligned} \mathrm{COD} &= 634.97 + 26.42\mathrm{A} + 17.92\mathrm{B} - 17.33\mathrm{C} - 10.63\mathrm{AB} \\ &\quad + 23.62\mathrm{AC} + 25.12\mathrm{BC} - 4.05\mathrm{A}^2 - 7.84\mathrm{B}^2 + 1.46\mathrm{C}^2 \end{aligned} \tag{1}$$

$$\mathrm{TSS} = 118.33 + 18\mathrm{A} + 9.98\mathrm{B} - 14.03\mathrm{C} - 6.50\mathrm{AB} + 15.25\mathrm{AC} + 19.5\mathrm{BC} \tag{2}$$

3.8 Analysis of response surface and determination of optimal value

Optimization minimizes the materials used during the experiment while maximizing the COD and TSS results. This approach is intended to reduce costs and time while achieving high treatment results to meet the objectives. Figures 11 and 12 display the plotting of the

Table 9 Comparison between the experimental and predicted data

Run	A: KOH-AC (g)	B: TiO_2 (g)	C: Clay (g)	Predicted values		Experimental values		Residuals	
				TSS (mg/l)	COD (mg/l)	TSS (mg/l)	COD (mg/l)	TSS (mg/l)	COD (mg/l)
1	3	0.55	1.25	120.15	637.18	119	635	1.15	2.18
2	1	1	0.5	132.40	639.86	130	639	2.40	0.86
3	5	0.1	0.5	155.25	659.22	156	659	-0.75	0.22
4	3	0.55	1.25	120.15	637.18	119	635	1.15	2.18
5	1	0.1	0.5	126.57	638.75	127	639	-0.85	-0.25
6	3	1.30681	1.25	137.55	644.17	135	642	2.55	2.17
7	5	1	0.5	114.18	633.06	115	631	-0.82	2.06
8	5	1	2	168.28	686.37	167	687	1.28	-0.63
9	3	0.55	1.25	120.15	637.18	119	635	1.15	2.18
10	6.36359	0.55	1.25	143.00	670.23	145	667	-2.00	3.23
11	5	0.1	2	110.87	630.62	112	629	-1.13	1.62
12	3	0.55	2.51134	92.31	613.23	91	609	1.31	4.23
13	1	0.1	2	42.30	501.45	40	500	1.45	1.45
14	1	1	2	102.45	617.83	103	615	2.83	-0.55
15	3	0.55	1.25	120.15	637.18	119	635	1.15	2.18
16	3	0.55	1.25	120.15	637.18	119	635	1.15	2.18
17	3	0.55	1.25	120.15	637.18	119	635	1.15	2.18

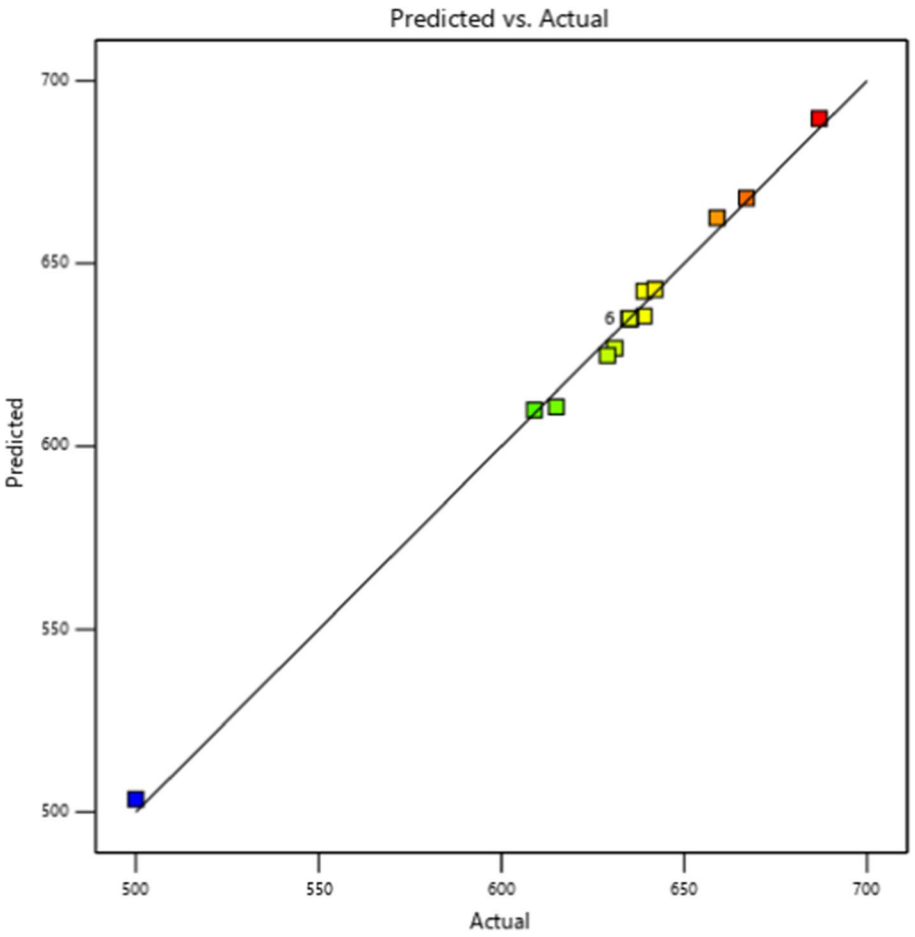

Fig. 9 Residual normal probability plot for COD

3D response surface, which shows the influence of the variables (independent), specifically the KOH-AC, TiO_2, and clay (MMT)**.** Based on the findings, the optimal values of KOH-AC loading of 1wt%, 0.628wt% of TiO_2 load, and 2wt% clay load to achieve the lowest COD and TSS values of 547.074 and 77.289 mg/L in POME. Extending the number of materials beyond these values will raise costs, resulting in lower profitability.

4 Conclusion

To conclude, Dabai can successfully produce a nanocomposite material for the adsorbent application. It is due to the presence of functional groups such as hydroxyl, phenolic, amide, and carbonyl on the surface of its nutshell, which provides strong adsorbent properties. Apart from good adsorbent properties, biodegradable material can also reduce solid waste production once it has reached its lifespan. When the developed nanocomposites are applied to the samples, the turbidity and pH values of POME are

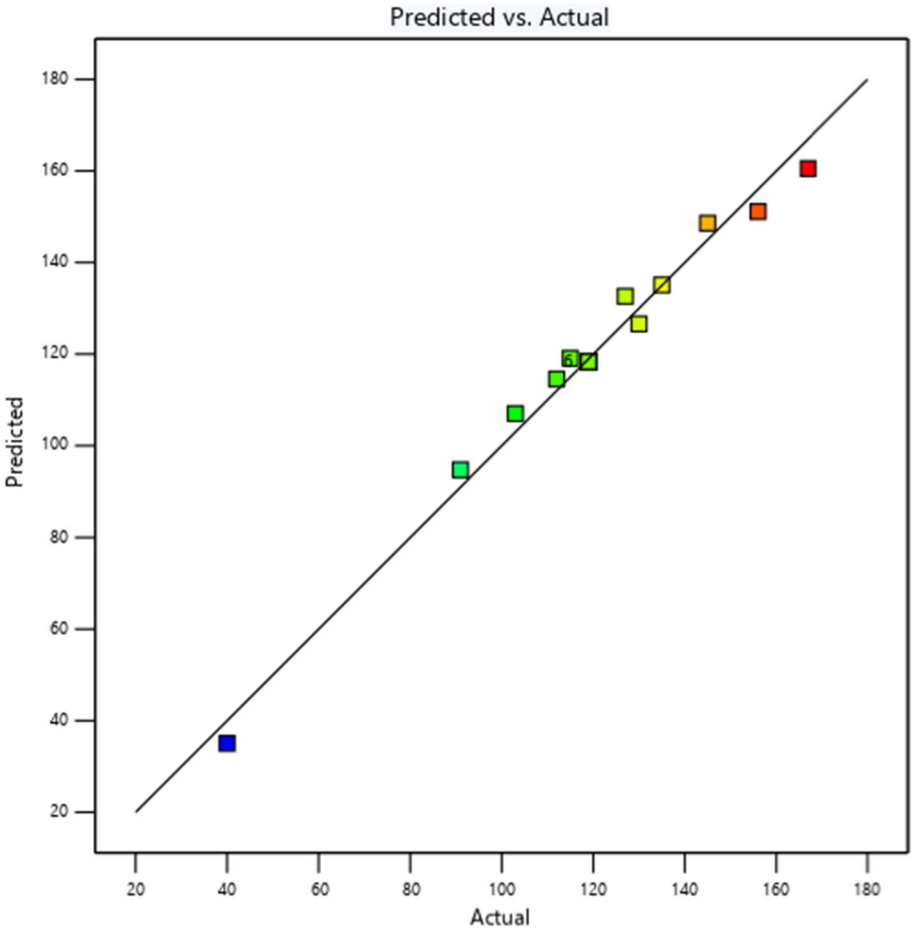

Fig. 10 Residual normal probability plot for TSS

reduced from their initial values. COD and TSS analyses confirmed the effectiveness of the nanocomposites powder, and the optimal composition of AC/TiO_2/MMT clay is designed using the Design Expert software, which indicates that using 1wt% KOH-AC, 0.628wt% TiO_2, and 2wt% clay loads will give the greatest COD and TSS reduction. Based on the result obtained from AAS analysis, the concentration of heavy metals such as Zn and Pb in POME has been successfully reduced by 86.7% and 97.3%. It is concluded that the composition of nanocomposites is a crucial factor that influences composites. The pore structure, adsorption capacity, and formation of active sites on the nanocomposite are believed to have an excellent result in minimizing environmental problems caused by POME discharge. Thus, the aim and objectives of the research are achieved, and the outcome has proved that Dabai-based activated carbon has great potential in treating POME.

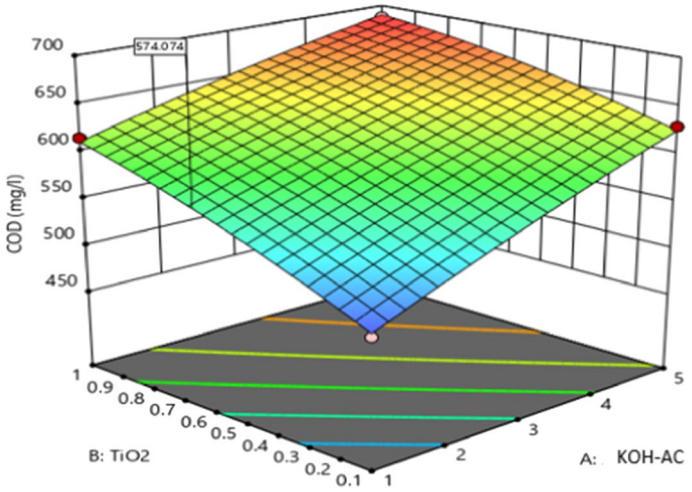

Fig. 11 Optimization plot for COD

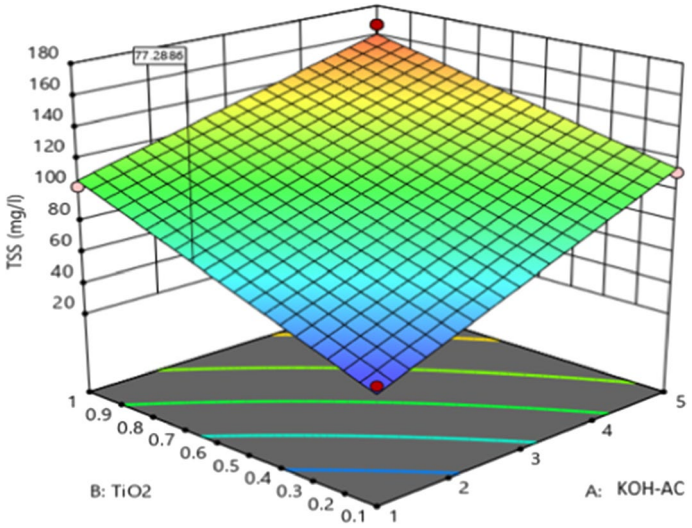

Fig. 12 Optimization plot of TSS

Acknowledgements The author wishes to express most sincere appreciation and deepest gratitude to the Department of Chemical Engineering and Energy Sustainability, Faculty of Engineering, Universiti Malaysia, Sarawak.

Data availability The authors confirm that the data supporting the findings of this study are available within the article [and/or] its supplementary materials.

Declarations

Conflict of interest The authors declare that they have no known competing financial interests or personal relationships that could have appeared to influence the work reported in this paper.

References

Abu-Danso, E., Peraniemi, S., Leiviska, T., & Kim, T. (2019). Synthesis of clay-cellulose biocomposite for the removal of toxic metal ions from aqueous medium. *Journal of Hazardous Materials*.

Adeleke, A., Abdul Latiff, A., Daud, Z., Mat Daud, N., & Aliyu, M. (2017). Heavy metal removal from wastewater of palm oil mill using develped activated carbon from coconut shell and cow bones. *Key Engineering Materials.*

Affam, A., & Bistar, A. (2020). Oxidation of palm oil mill effluent using hydrogen peroxide and catalysed by UV/light/zinc oxide. *IOP Conference Series: Materials Science and Engineering*. https://doi.org/10.1088/1757-899X/736/4/042025

Ahmad, A., & Azam, T. (2019). Water purification technologies. *Bottled and Packaged Water*.

Ahrouch, M., Gatica, J., Draoui, K., & Vidal, H. (2019). Adding value to natural clays as low-cost adsorbents of methylene blue in polluted water through honeycomb monoliths manufacture. *SN Applied Sciences*. https://doi.org/10.1007/s42452-019-1636-4

Akhbarizadeh, R., Moore, F., Mowla, D., & Keshavarzi, B. (2018). Improved waste-sourced biocomposite for simultaneous removal of crude oil and heavy metals from synthetic and real oilfield-produced water. *Environmental Science and Pollution Research*. https://doi.org/10.1007/s11356-018-3136-2

Alhaji, M., Sanaullah, K., Lim, S., Rigit, A., Hamza, A., & Khan, A. (2017). Modeling and optimisation of photocatalytic treatment of pre-treated palm oil mill effluent (POME) in a UV/TiO2 system using response surface methodology (RSM). *Cogent Engineering*. https://doi.org/10.1080/23311916.2017.1382980

Amosa, M., Jam, M. S., Alkhatib, M., Tajari, T., Jimat, D. N., & Owolabi, R. (2016). Turbidity and suspended solids removal from high-strength wastewater using high surface are adsorbent: mechanistic pathway and statistical analysis. *Cogent Engineering*. https://doi.org/10.1080/23311916.2016.1162384

Arjmandi, R., Hassan, A., Haafiz, M. M., & Zakaria, Z. (2016). Effects of micro and nano-cellulose on tensile and morphological properties of montmorilloite nanoclay reinforced polylactic acid nanocomposites. *Nanoclay reinforced polymer composites* (pp. 103–125). Springer.

ASTM E1252–98. (2021). Standard practice for general techniques for obtaining infrared spectra for qualitative analysis, ASTM International, West Conshohocken, PA. Retrieved from HYPERLINK "https://www.astm.org/" www.astm.org

ASTM E168–16. (2016). Standard practices for general techniques of infrared quantitative analysis, ASTM International, West Conshohocken, PA. Retrieved from Hyperlink "https://www.astm.org/" www.astm.org

ASTM E2015–04. (2014). Standard guide for preparation of plastics and polymeric specimens for microstructural examination, ASTM International, West Conshohocken, PA.

Azadi, S., Karimi-Jashni, A., Javadpour, S., & Mahmoudian-Boroujerd, L. (2020). Photocatalytic landfill leachate treatment using P-type TiO2 nanoparticles under visible light irradation. *Environment, Development and Sustainability*. https://doi.org/10.1007/s10668-020-00861-4

Bansal, P., Bui, T., & Lee, B.-K. (2019). Potential applications of ASR fly ash in photo-Fenton like process for the degradation of tetracyclineat neutral pH: Fixed-bed approach. *Chemical Engineering Journal*. https://doi.org/10.1007/s10668-020-00861-4

Behera, S. K., Meena, H., Chakraborty, S., & Meikap, B. (2018). Application of response surface methodology (RSM) for optimization of leaching parameters for ash reduction from low-grade coal. *International Journal of Mining Science and Technology, 28*, 621–629.

Bozorg-Haddad, O., Delpasand, M., & Loaiciga, H. A. (2021). Water quality, hygiene and health. *Economical, Political, and Social Issues in Water Resources*.

Briffa, J., Sinagra, E., & Blundell, R. (2020). Heavy metal pollution in the environment and their toxicological effects on humans. *Heliyon*. https://doi.org/10.1016/j.heliyon.2020.e04691

Bui, T., Bansal, P., Lee, B.-K., & Mahvelati-Shamsabadi, T. (2019). Facile fabrication of novel Ba-doped g-C3N4 photocatalyst with remarkably enhanced photocatalytic activity towards tetracycline elimination under visible-light irradiation. *Applied Surface Science*. https://doi.org/10.1016/j.apsusc.2019.144184

Chakravarty, P., & Kumar, M. (2019). Floral species in pollution remediation and augmentation of micro-meteorological conditions and microclimate. *Phytomanagement of Polluted Sites*. https://doi.org/10.1016/B978-0-12-813912-7.00006-5

Charles, A., Khan, M., Ng, K., Wu, T., Lim, J., Wongsakulpasatch, S., Witoon, T., & Cheng, C. (2019). Facile synthesis of CaFe2O4 for visible light driven treatment of polluting palm oil mill effluent: Photokinetic and scavenging study. *Science of the Total Environment*. https://doi.org/10.1016/j.scitotenv.2019.01.195

Chkirida, S., Zari , N., Qaiss, E., & Bouhfid , R. (2019). Nanocomposite materials based of TiO2/ clay for wastewater treatment. *SpringerBriefs in Information Systems*.

Chikri, R., Elhadiri, N., Benchana, M., & Maguana, Y. (2020). Efficiency of sawdust as low-cost adsorbent for dye removal. *Journal of Chemistry*. https://doi.org/10.1155/2020/8813420

Chobchun, M., Jutakridsada, P., Thiamsinsangwon, P., Kasemsiri, P., Kamwilaisak, K., & Chindaprasirt, P. (2020). Characterization of Tio2-activated carbon onto adsorption and photocatalytic properties and its application. *Journal of Metals, Materials and Minerals*. https://doi.org/10.55713/jmmm.v30i4.833

Daneshpayeh, S., Ghasemi, F. A., Ghasemi, I., & Ayaz, M. (2016). Predicting of mechanical properties of PP/LLDPE/TiO2 nanocomposites by response surface methodology. *Composites Part B: Engineering*. https://doi.org/10.1016/j.compositesb.2015.08.075

Edokpayi, J. N., Odiyo, J. O., & Durowoju, O. S. (2017). Impact of wastewater on surface water quality in developing countries: A case study of South Africa. *Water Quality*, pp. 401–416.

Eskandari, P., Farhadian, M., Nazar, A. S., & Jeon, B.-H. (2019). Adsorption and photodegradation efficiency of TiO2/Fe2O3/PAC and TiO2/Fe2O3/Zeolite nanophotocatalysts for removal of cyanide. *Industrial & Engineering Chemistry Research*. https://doi.org/10.1021/acs.iecr.8b05073

Fausey, C., Zucker, I., Shaulsky, E., Zimmerman, J., & Elimelech, M. (2019). Removal of arsenic with reduced graphene oxide-TiO2-enabled nanofibrous mats. *Chemical Engineering*. https://doi.org/10.1016/j.cej.2019.122040

Gisi, S., Lofrano, G., Grassi, M., & Notarnicola, M. (2016). Characteristics and adsorption capacities of low-cost sorbents fro wastewater treatment: A review. *Sustainable Materials and Technologies*. https://doi.org/10.1016/j.susmat.2016.06.002

Hassan, N. A., Jun, C. H., Razak, A., Afandi, M., Sani, M., & Aidin, M. (2019). Physicochemical, microbiological and sensory properties of dabai cake. *Journal of Sciences and Technology*, 69–73.

Jagaba, A., Kutty, S., Hayder, G., Baloo, L., Ghaleb, A., Lawal, I., & Umaru , I. (2020). Degradation of Cd, Cu, Fe, Mn, Pb, and Zn by Moringa-oleifera, zeolite, ferric-chloride, chitosan and alum in an industrial effluent. *Ain Shams Engineering Journal.*

James, A., Rahman, M., Huda, D., Aqlan, F., Matin, M., Bakri, M., Kuok, K., & Rahman, M. (2022). Synthesis and characterization of novel nano-carbon mixture from Dabai (Canarium odontophyllum) nutshell. *BioResources*. https://doi.org/10.15376/biores.17.3.4452-4469

Kaman, S. P., Tan, I. W., & Lim, L. (2017). Palm oil mill effluent treatment using coconut shell-based activated carbon: Adsorption equilibrium and isotherm. *MATEC Web of Conferences*, (p. 87).

Kamil, F., Haasanuddin, N. I., Othman, R., & Anuar, F. (2020). Treatment of palm oil mill effluent by poly(L-lactic acid)-poly (ethylene glycol)/ silica membrane. *Sains Malaysiana*.

Kamyab, H., Chelliapan, S., Din, M. M., Lee, C. T., Rezania, S., Khademi, T., & Bong, C. (2018). Isolate new microalgal strain for biodiesel production and using FTIR spectroscopy for assessment of pollutant removal from palm oil mill effluent (POME). *Chemical Engineering Transactions*.

Kanakaraju, D., Ahmad, N., Sedik, N., Long, S., Guan, T., & Chin, L. (2017). Performance of solar photocatalysis and photo-Fenton degradation of palm oil mill effluent. *Malaysian Journal of Analytical Sciences*. https://doi.org/10.17576/mjas-2017-2105-01

Karoui, S., Arti, R. B., Mougin, K., Ghorbal, A., Assadi, A., & Amrane, A. (2019). Synthesis of novel biocomposite powder for simultaneous removal of hazardous ciprofloxacin and methylene blue: Central composite design, kinetic and isotherm studies using Brouers-Sotolongo family models. *Journal of Hazardous Materials*.

Khan, S., & Ali, J. (2018). Chemical analysis of air and water. *Bioassays Advanced Methods and Applications*, pp. 21–39.

Koohestanian, A., Hosseini, M., & Abbasian, Z. (2008). The separation method for removing of colloidal particles from raw water. *American-Eurasian Journal of Agricultural and Environmental Sciences*.

Kothari, V., Vij, S., Sharma, S., & Gupta, N. (2017). Correlation of various water quality parameters and water quality index of districts of Uttarakhand. *Environmental and Sustainability Indicators*.

Kuang, Y., Zhang, X., & Shaoqi, Z. (2020). Adsorption of methylene blue in water onto activated carbon by surfactant modification. *Water*. https://doi.org/10.3390/w12020587

Kusiak-Nejman, E., Moszynski, D., Kapica-Kozar, J., Wanag, A., & Morawski, A. (2018). Assessment of the suitability of the one-step hydrothermal method for preparation of non-covalently/covalently-bonded TiO2/graphene-based hybrids. *Nanomaterials*. https://doi.org/10.3390/nano8090647

Lazaratou, C. V., Vayenas, D. V., & Papoulis, D. (2020). The role of clays, clay minerals and clay-based materials for nitrate removal from waste system: A Review. *Applied Clay Science, 185*(1), 105377. https://doi.org/10.1016/j.clay.2019.105377

Lellis, B., Favaro-Polonio, C., Pamphile, J., & Polonio, J. (2019). Effects of textile dyes on health and the environment and bioremediation potential of living organisms. *Biotechnology Research and Innovation*. https://doi.org/10.1016/j.biori.2019.09.001

Leon, A., Reuquen, P., Garin, C., Segura, R., Vargas, P., Zapata, P., & Orihuela, P. A. (2016). FTIR and raman characterization of TiO2 nanoparticles coated with polyethylene glycol as carrier for 2-methoxyestradiol. *Applied Sciences*. https://doi.org/10.3390/app7010049

Lim, A., Chew, J. J., Ngu, L. H., Ismadji, S., Khaerudini, D. S., & Sunarso, J. (2020). Synthesis, characterization, adsorption isotherm and kinetic study of oil palm trunk-derived activated carbon for tannin removal from aqueous solution. *ACS Omega*. https://doi.org/10.1021/acsomega.0c03811

Maguana, Y. E., Elhadiri, N., Bouchdoug, M., Benchanaa, M., & Jaouad, A. (2019). Activated carbon from prickly ear seed cake: Optimization of preparation conditions using experimental design and its application in dye removal. *International Journal of Chemical Engineering*, *12*.

Mannaa, M., Qasim, K., Alshorifi, F. T., El-Bahy, S. M., & Salama, R. (2021). Role of NiO nanoparticles in enhancing structure properties of TiO2 and its applications in photodegration and hydrogen evolution. *ACS Omega*. https://doi.org/10.1021/acsomega.1c03693

Mohammed, S. S. (2015). Effect of pH on the turbidity removal of wastewater. *Scientific Research*.

Mohammad, S., Baidurah, S., Kobayashi, T., Ismail, N., & Leh, C. P. (2021). Palm oil mill effluent tretament processes. *Processes*. https://doi.org/10.3390/pr9050739

Mopoung, S., Moonsri, P., Palas, W., & Khumpai, S. (2015). Characterization and properties of activated carbon prepared from tamarind seeds by KOH activation for FE (III) adsorption from aqueous solution. *The Scientific World Journal*. https://doi.org/10.1155/2015/415961

Ng, K. H., Khan, M., Ng, Y., Hossain, S., & Cheng, C. (2017). Restoration of liquid effluent from oil palm agroindustry in Malaysia using UV/TiO2 and UV/ZnO photocatalytic systems: A comparative study. *Journal of Environmental Management*. https://doi.org/10.1016/j.jenvman.2017.03.078

Ng, K., & Cheng, C. (2017). Photocatalytic degradation of palm oil mill effluent over ultraviolet-responsive titania: Successive assessments of significance factors and process optimization. *Journal of Cleaner Production*. https://doi.org/10.1016/j.jclepro.2016.11.077

Nguyen-Dinh, M.-T., Bui, T., Bansal, P., Jourshabani, M., & Lee, B.-K. (2021). Photocatalytic and photo-electrochemical behavior of novel SnO_2-modified-g-C_3N_4 for complete elimination of tetracycline under visible-light irradiation: Slurry and fixed-bed approach. *Separation and Purification Technology*. https://doi.org/10.1016/j.seppur.2021.118607

Osman, N., Ujang, F., Roslan, A., Ibrahim, M., & Hassan, M. (2020). The effect of palm oil mill effluent final discharge on the characteristics of Pennisetum Purpureum. *Scientific Reports*.

Pant, B., Pant, H., & Park, M. (2020). Fe1-xS modified TiO2 NPs embedded carbon nanofiber composite via electrospinning: A potential electrode material for supercapacitors. *Molecules*.

Popoola, L. T. (2019). Nano-magnetic walnut shell-rice husk for Cd (II) sorption: Design expert and optimization using artificial intelligence and design expert. *Heliyon*.

Reghunanth, S., Pinheiro, D., & Devi, K. R. S. (2021). A Review of hierrachiral nanostructures of TiO2: Advances and Applications. *Applied Surface Science Advances, 3*(1), 100063. https://doi.org/10.1016/j.apsadv.2021.100063

Reza, M., Yun, C., Afroze, S., Radenahmad, N., Bakar, M., Saidur, R., & Azad, A. (2020). Preparation of activated carbon from biomass and its applications in water and gas purification. *Arab Journal of Basic and Applied Sciences*. https://doi.org/10.1080/25765299.2020.1766799

Saleem, J., Shahid, U. B., Hijab, M., Mackey, H., & Mckay, G. (2019). Production and applicatios of activated carbons as adsorbents from olive stone. *Biomass Conversion and Biorefinery*. https://doi.org/10.1007/s13399-019-00473-7

Saputera, W., Amri, A., Mukti, R., Suendo, V., Devianto, H., & Sasongko, D. (2021). Photocatalytic degradation of palm oil mill effluent (POME) waste using $BiVO_4$ based catalysts. *Molecules*. https://doi.org/10.3390/molecules26206225

Scholz, M. (2016). Constructed wetlands. *Wetlands for Water Pollution Control (Second Edition)*.

Shahrifun, N. S. (2015). Characterization of palm oil mill secondary effluent (POMSE). *KSCE Journal of Civil Engineering*.

Sia, Y. Y., Tan, I. A., & Abdullah, M. O. (2016). Adsorption of colour, TSS and COD from palm oil mill effluent (POME) using acid-washed coconut shell activated carbon: kinetic and mechanism studies. *MATEC Web of Conference* (p. 87). Kota Samarahan: ENCON.

Srivatsav, P., Bhargav, B. S., Shanmugasundaram, V., Arun, J., Gopinath, K. P., & Bhatnaga, A. (2020). Biochar as an eco-friendly and economical adsorbent for the removal of colorants (dyes) from aqueous environment: A review. *Adsorbents Fro Water and Wastewater Treatment and Resource Recovery*. https://doi.org/10.3390/w12123561

Taoufik, N., Elmchaouri, A., Anouar, F., Korili, S., & Gil, A. (2019). Improvement of the adsorption properties of an activated carbon coated by titanium dioxide for the removal of emerging contaminants. *Journal of Water Process Engineering*. https://doi.org/10.1016/j.jwpe.2019.100876

Tian, F., Wu, Z., Yan, Y., Ye, B.-C., & Liu, D. (2016). Synthesis of visible-light-responsive Cu and N-Codoped AC/TiO2 photocatalyst through microwave irradiation. *Nanoscale Research Letters*. https://doi.org/10.1186/s11671-016-1503-9

Ukanwa, K. S., Patchigolla, K., Sakrabani, R., Anthony, E., & Mandavgane, S. (2019). A review of chemicals to produce activated carbon from agricultural waste biomass. *Sustainability*. https://doi.org/10.3390/su11226204

Zahari, M. I., Baharum, A., Anuar, F., & Othaman, R. (2017). Palm oil industry in South East Asia and the effluent treatment technology. *Environmental Technology & Innovation*.

Zainuri, N., Hairom, N., Sidik, D., Desa, A., Misdan, N., Yusof, N., & Mohammad, A. (2018). Palm oil mill secondary effluent (POMSE) treatment via photocatalysis process in presence of ZnO-PEG nanoparticles. *Journal of Water Process Engineering*. https://doi.org/10.1016/j.jwpe.2018.08.009